Journal of Nanobiotechnology

RESEARCH

Open Access

Atherosclerosis enhances the efficacy of liposome-encapsulated bromocriptine in reducing the incidence of prolactinemia in pituitary tumors

Zhe Zhang[1,3,4,5,6†], Guangyu Jia[1,3,4,5,6†], Qi Wang[1,3,4,5,6†], Yamei Yu[2,3,4,5,6], Xiaolong Tang[1,3,4,5,6], Heqing Zheng[2,4,5,6], Xinyu Yang[2,4,5,6], Yao Xiao[1,3,4,5,6], Yangrui Ou[1,3,4,5,6], Jingjing Jiang[1,3,4,5,6], Hua Guo[1,3,4,5,6*], Ye Wang[2,3,4,5,6*] and Shiyong Li[1,3,4,5,6*]

Abstract

Intranasal drug delivery via nanocarriers has long been a research focus for enhancing drug concentration in the brain. However, the strategy of exploiting blood–brain barrier (BBB) alterations in atherosclerotic mouse models to enhance nanoparticle-mediated delivery of bromocriptine to the hypothalamus for the treatment of prolactinomas with hyperprolactinemia has not yet been reported. This study reveals that in patients with prolactinomas complicated by arteriosclerosis, bromocriptine therapy more effectively attenuates postoperative elevations in prolactin levels. In a mouse model, liposome-encapsulated bromocriptine efficiently traversed the nasal mucosa and entered the intracranial space. Compared with normal mice, bromocriptine-loaded liposomes delivered higher bromocriptine concentrations to the hypothalamus. Single-cell RNA sequencing revealed a significant upregulation of organic anion-transporting polypeptide 1a4 (Oatp1a4) expression in the brain endothelial cells of atherosclerotic mice. Importantly, bromocriptine-loaded liposomes more effectively reduced prolactin levels in a mouse model of prolactinoma with concurrent atherosclerosis. This study provides a theoretical foundation for the precision treatment of prolactinomas in arteriosclerosis.

†Zhe Zhang, Guangyu Jia and Qi Wang equally contributed to this work.

*Correspondence:
Hua Guo
ndefy02014@ncu.edu.cn
Ye Wang
ndefy08041@ncu.edu.cn
Shiyong Li
sylicg@ncu.edu.cn

Full list of author information is available at the end of the article

Graphical Abstract

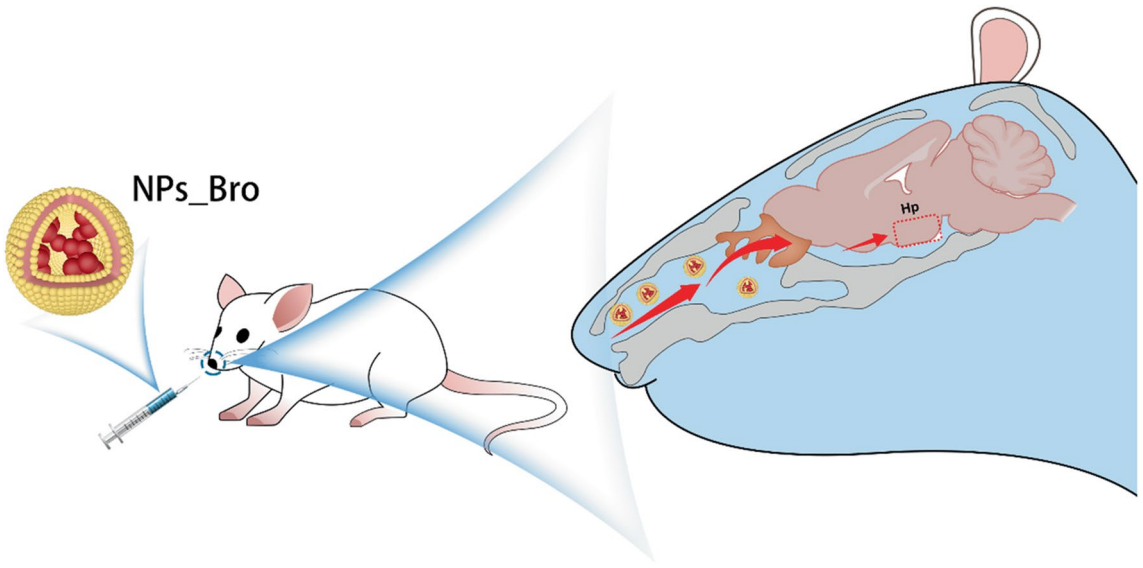

Keywords Atherosclerosis, Bromocriptine, Prolactinoma, OATP transporter

Introduction

Pituitary tumors with concomitant hyperprolactinemia are common endocrine disorders, with prolactinomas accounting for approximately 30–50% of all pituitary adenomas [1]. The hallmark of this condition is a significant elevation of serum prolactin (PRL) levels [2]. Prolactinomas are more prevalent in females, with an estimated incidence of 15 to 20 cases per 100,000 individuals [3]. Bromocriptine (2-bromo-α-ergocryptine mesylate), a semi-synthetic ergot alkaloid and dopamine receptor agonist, effectively reduces prolactin levels and shrinks tumor size in most patients [4–6]. However, bromocriptine treatment is often associated with adverse effects such as nausea, headaches, and dizziness, leading some patients to discontinue therapy. Additionally, these side effects, along with the necessity for long-term medication use, may compromise patient adherence and ultimately reduce therapeutic efficacy. Therefore, developing safe and effective treatment strategies that improve patient compliance, including optimized drug formulations and advanced drug delivery systems is crucial [7].

The blood-brain barrier (BBB) serves as a natural protective barrier regulating the passage of substances between the cerebrospinal fluid and brain tissue, posing a significant challenge for the treatment of central nervous system (CNS) disorders [8–10]. Intranasal drug delivery has been explored as an effective approach to enhance drug transport across the BBB and increase drug concentrations within the brain [11, 12]. Liposomes, composed of phospholipid bilayers, are widely utilized in drug delivery systems due to their ability to encapsulate drugs, improve bioavailability, and mitigate adverse effects [13–15]. However, our study focuses on leveraging the inherent advantages of intranasal liposomal drug delivery and the structural and functional changes in the BBB to achieve efficient intracerebral drug targeting and precision therapy for patients.

Atherosclerosis is a chronic inflammatory disease characterized by lipid deposition in the arterial wall, infiltration of inflammatory cells, and fibrosis, accompanied by alterations in vascular endothelial function and tight junction protein expression. These changes can modulate the permeability of the BBB [16, 17]. However, whether liposome-encapsulated bromocriptine can more effectively traverse the atherosclerosis-altered BBB and enhance the therapeutic efficacy against prolactinomas remains unclear. Here, our data demonstrate that in patients with prolactinomas and concurrent arteriosclerosis, bromocriptine treatment more effectively reduces the incidence of postoperative hyperprolactinemia. Moreover, in atherosclerotic mice, the BBB exhibits increased permeability to bromocriptine, leading to enhanced suppression of prolactin levels. This study provides a theoretical foundation for precision therapy in patients with prolactinomas and coexisting arteriosclerosis.

Results and discussions

In patients with arteriosclerosis, bromocriptine more effectively reduces the recurrence rate of hyperprolactinemia

Given that atherosclerosis can alter blood-brain barrier (BBB) permeability [18], we investigated whether

bromocriptine can better traverse the BBB and improve treatment outcomes for prolactinomas, providing a basis for precision therapy in prolactinoma management. First, we conducted a retrospective analysis of patients with pituitary tumors who underwent surgical treatment at the Neurosurgery Department of the Second Affiliated Hospital of Nanchang University between January 2018 and December 2023 (Supplementary Fig. 1). As shown in Fig. 1A-B, patients were divided into an arteriosclerosis group and a non-arteriosclerosis group based on fundus photography [19, 20]. The baseline characteristics of the two groups, including age, tumor size, bromocriptine use, and prolactin levels, were similar prior to surgery (Table 1). To control for the influence of clinical characteristics on surgical outcomes, we balanced the baseline factors between the two groups, including age, tumor size, medication duration, and preoperative prolactin levels. Notably, the age difference between the arteriosclerosis group (46.7 ± 13.73 years, $n = 7$) and the non-arteriosclerosis group (46.6 ± 13.99 years, $n = 16$) was not statistically significant (Fig. 1C). Tumor size, with an average maximum diameter of 2.0 ± 0.70 cm and minimum diameter of 1.4 ± 0.56 cm in the arteriosclerosis group and an average maximum diameter of 2.1 ± 0.98 cm and minimum diameter of 1.4 ± 0.68 cm in the non- arteriosclerosis group, showed no significant differences, indicating comparable tumor volumes between the two groups (Fig. 1D-E). The treatment duration for bromocriptine was 10.3 ± 7.73 months in the arteriosclerosis group and 12.3 ± 10.50 months in the non- arteriosclerosis group, with no significant difference (Fig. 1F). Preoperative prolactin levels were similar between the arteriosclerosis group (102.5 ± 68.51 ng/mL) and the non-arteriosclerosis group (106.9 ± 68.26 ng/mL). However, unlike the non-arteriosclerosis group, serum prolactin levels in the arteriosclerosis group returned to the normal range on the first postoperative day (Fig. 1G-H). These findings suggest that preoperative bromocriptine administration significantly improved the cure rate in prolactinoma patients with concomitant retinal arteriosclerosis. Furthermore, these results imply that bromocriptine may more readily cross the blood-brain barrier to reach the hypothalamus.

Both free Bromocriptine and nanoparticle-encapsulated bromocriptine exhibit limited transendothelial penetration from the abluminal side of blood vessels

Previous studies have demonstrated that liposomes can efficiently encapsulate bromocriptine [21, 22]. We prepared bromocriptine-loaded lipid nanoparticles using a film hydration method combined with ultrasonication, resulting in particles with a size of 123.6 ± 10.6 nm and a zeta potential of -7.6 ± 1.9 mV (Supplementary Fig. 2A-B). The bromocriptine liposome nanoparticles exhibited excellent stability in DMEM culture medium with 10% fetal calf serum (FCS) at 37 °C (Supplementary Fig. 2C).

To investigate the effect of atherosclerotic BBB on bromocriptine permeability, we established an in vitro atherosclerotic BBB model using oxidized low-density lipoprotein (ox-LDL) and human cerebral microvascular endothelial cells (HCMEC/D3) [23]. We applied the drugs to the outer side of the vascular wall to analyze their ability to cross the vessel wall. The experimental results showed that, compared to the normal BBB model, both free bromocriptine and liposome-loaded bromocriptine nanoparticles permeated the endothelial cell layer from the outer side of the vascular wall to a lesser extent in the atherosclerotic BBB model (Fig. 2A). Furthermore, there was no significant statistical difference in the permeability between free bromocriptine and nanocarrier-loaded bromocriptine in the atherosclerotic BBB model (Fig. 2B). These results suggest that bromocriptine crosses the atherosclerotic BBB model to a lesser extent, entering the inner side of the vascular wall.

Atherosclerosis enhances the delivery of bromocriptine-loaded nanoparticles to the hypothalamus

Intranasal drug delivery offers unique advantages for brain drug delivery, as the drug can be absorbed through the nasal mucosa and directly enter the cerebrospinal fluid (CSF) and brain tissue [24, 25]. Liposomes, when administered intranasally, can enhance drug absorption, protect drug stability, and improve brain targeting, showing great potential in treating central nervous system disorders [26]. In this study, after intranasal administration of free bromocriptine and bromocriptine-loaded nanocarriers, we assessed the distribution of bromocriptine in the nasal mucosa and brain tissue of mice. We quantified the drug concentrations (Fig. 3A). The results showed that, after 120 min of intranasal administration, bromocriptine-loaded lipid nanoparticles exhibited significant accumulation in the nasal mucosa region of atherosclerotic model mice (Fig. 3B-C). The fluorescence intensity of rhodamine-modified bromocriptine-loaded nanoparticles was significantly higher than that of free rhodamine, indicating that the lipid nanoparticles enhanced brain drug delivery.

Furthermore, we measured bromocriptine concentrations in the hypothalamus of different drug groups after intranasal administration using HPLC. In the wild-type mice and Apoe-/- mice administered free bromocriptine, the concentrations were 2.01 ± 0.05 ng/mg and 2.18 ± 0.07 ng/mg, respectively. These levels were significantly lower than those observed in the corresponding groups receiving nanoparticle-loaded bromocriptine, where the concentrations reached 8.25 ± 1.28 ng/mg and 21.01 ± 1.28 ng/mg, respectively (Fig. 3D). These results suggest that lipid nanoparticles can enhance the delivery of

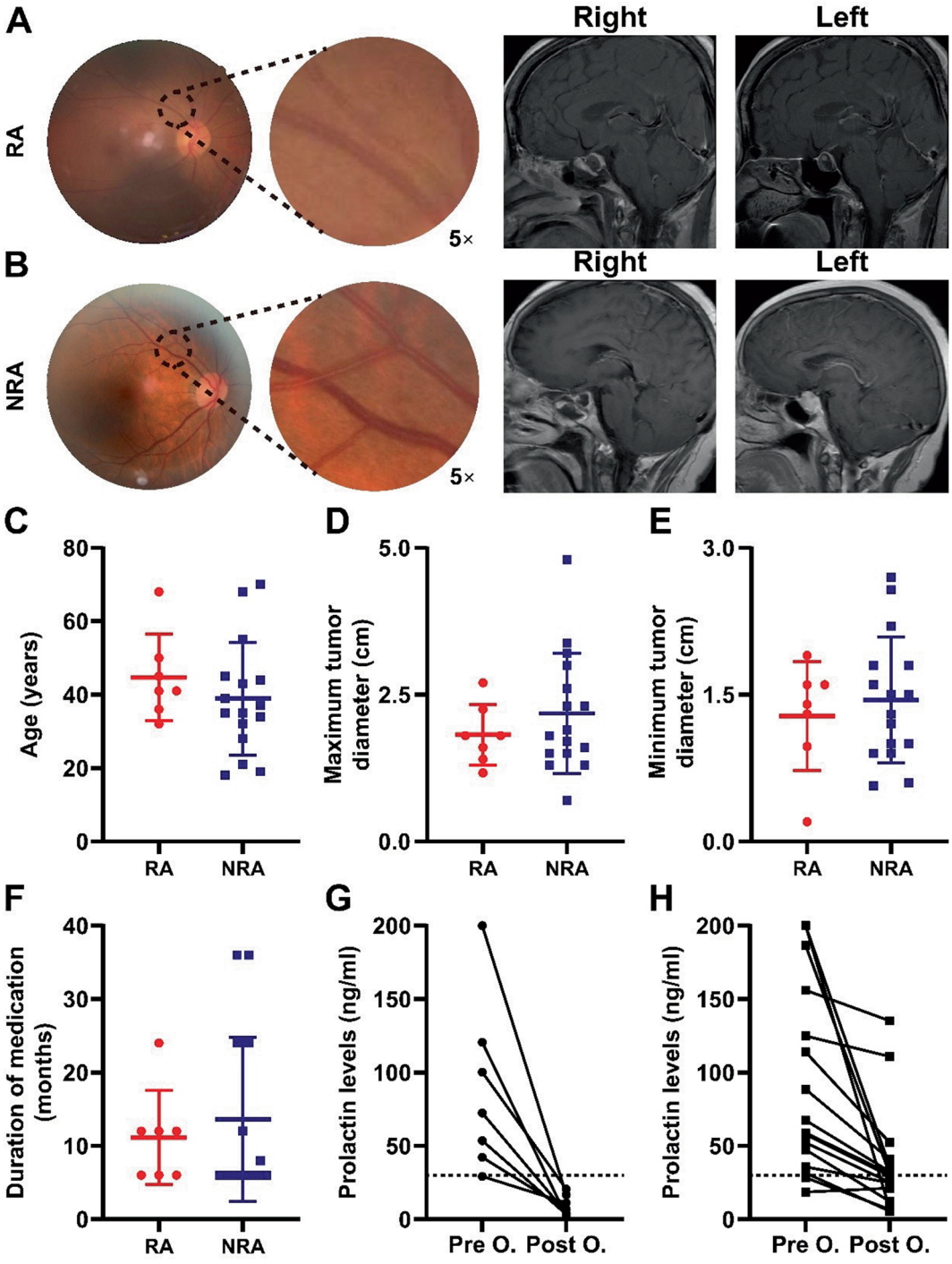

Fig. 1 Preoperative use of bromocriptine is more effective in patients with prolactinomas and concomitant retinal arteriosclerosis. (**A-B**) Representative visual field tests and pre-and post-operative contrast-enhanced brain MRI images of patients with retinal arteriosclerosis (**A**) and without retinal arteriosclerosis (**B**). (**C-F**) Comparative analysis of preoperative age (**C**), maximum tumor diameter (**D**), minimum tumor diameter (**E**), and duration of bromocriptine use (**F**) between the arteriosclerosis group ($n=7$) and non-arteriosclerosis group ($n=16$). Pre- and post-operative prolactin level changes in the arteriosclerosis group ($n=7$) (**G**) and non-arteriosclerosis group ($n=16$) (**H**). (RA, Retinal arteriosclerosis; NRA, Nonretinal arteriosclerosis; Pre O, preoperation; Post O, postoperation; Dashed line: Reference range for normal values)

Table 1 Baseline characteristics of all enrolled patients

Patients	Clinical Characteristic			Prolactin (ng/ml)		Tumor Size (cm)	
	Age	Sex	Fundus photography	Preoperative	Postoperative	Maximum diameter	Minimum diameter
Patient 1	50	Female	Retinal arteriosclerosis	53.53	3.42	1.6	0.2
Patient 2	41	Female	Retinal arteriosclerosis	100.21	20.52	2.7	1.6
Patient 3	36	Female	Retinal arteriosclerosis	200	16.72	1.8	1.6
Patient 4	41	Male	Retinal arteriosclerosis	120.64	2.31	1.4	1.3
Patient 5	45	Male	Retinal arteriosclerosis	72.37	4.4	1.17	0.97
Patient 6	68	Female	Retinal arteriosclerosis	42.2	6.74	2.25	1.9
Patient 7	32	Female	Retinal arteriosclerosis	29.3	11.27	1.8	1.4
Patient 8	39	Female	Nonretinal arteriosclerosis	200	36.17	4.8	2.7
Patient 9	34	Female	Nonretinal arteriosclerosis	124.99	110.87	1.5	0.9
Patient 10	35	Male	Nonretinal arteriosclerosis	28.35	6.8	2.6	1.5
Patient 11	44	Female	Nonretinal arteriosclerosis	58.94	31.18	2.3	1.8
Patient 12	28	Female	Nonretinal arteriosclerosis	156.11	135.22	1.6	0.6
Patient 13	32	Female	Nonretinal arteriosclerosis	35.8	24.91	1.3	1
Patient 14	37	Female	Nonretinal arteriosclerosis	57.69	29.6	1.9	1
Patient 15	19	Female	Nonretinal arteriosclerosis	113.96	52.48	0.7	0.57
Patient 16	21	Male	Nonretinal arteriosclerosis	52.26	25.31	1.3	0.9
Patient 17	19	Male	Nonretinal arteriosclerosis	200	7.22	3.38	2.57
Patient 18	35	Female	Nonretinal arteriosclerosis	67.39	32.55	3.2	2.2
Patient 19	68	Male	Nonretinal arteriosclerosis	47.38	12.21	1.7	1.6
Patient 20	70	Male	Nonretinal arteriosclerosis	18.6	21.23	3	1.8
Patient 21	45	Female	Nonretinal arteriosclerosis	186.53	31.1	2.3	1.5
Patient 22	43	Female	Nonretinal arteriosclerosis	31.56	5.52	1.8	1.2
Patient 23	55	Female	Nonretinal arteriosclerosis	88.61	40.88	1.5	1.3

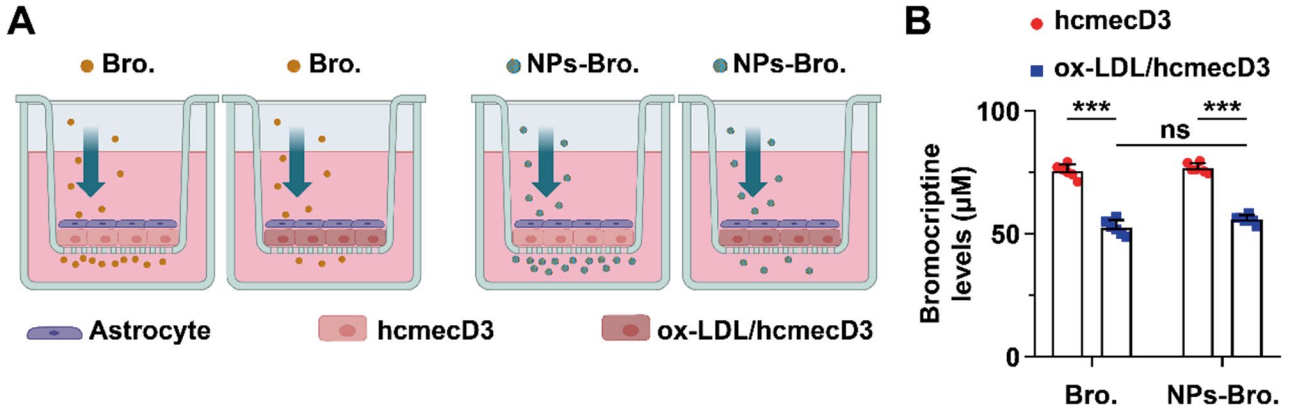

Fig. 2 Reduced permeability of bromocriptine and bromocriptine-loaded nanocarriers in the in vitro atherosclerotic BBB model. (**A**) Schematic of the in vitro atherosclerotic BBB model. (**B**) Quantitative analysis of the permeability of free bromocriptine and bromocriptine-loaded nanocarriers across the in vitro blood-brain barrier model. (NPs-Bro: Bromocriptine liposome nanoparticles) (*, $P < 0.05$; **, $P < 0.01$; ***, $P < 0.001$)

bromocriptine to the hypothalamus. Notably, compared to normal mice, bromocriptine-loaded lipid nanoparticles delivered more bromocriptine to the hypothalamus, indicating that the intranasal route significantly enhances the efficiency of nanocarrier-mediated targeted delivery of bromocriptine to the hypothalamus, with this effect being more pronounced in atherosclerotic model mice.

Construction of the single-cell transcriptomic atlas of cerebral vasculature in Sham and Apoe-/- mice

Following intranasal administration, a substantial amount of the drug enters the cerebrospinal fluid (CSF), with the arterial perivascular space serving as an important conduit for the drug's transport from the CSF into the brain parenchyma. To uncover the mechanisms by which atherosclerosis facilitates intranasal drug delivery, we utilized single-cell RNA sequencing (scRNA-seq) to investigate the cellular diversity and functional differences in the arterial vessel walls [27, 28]. In this study,

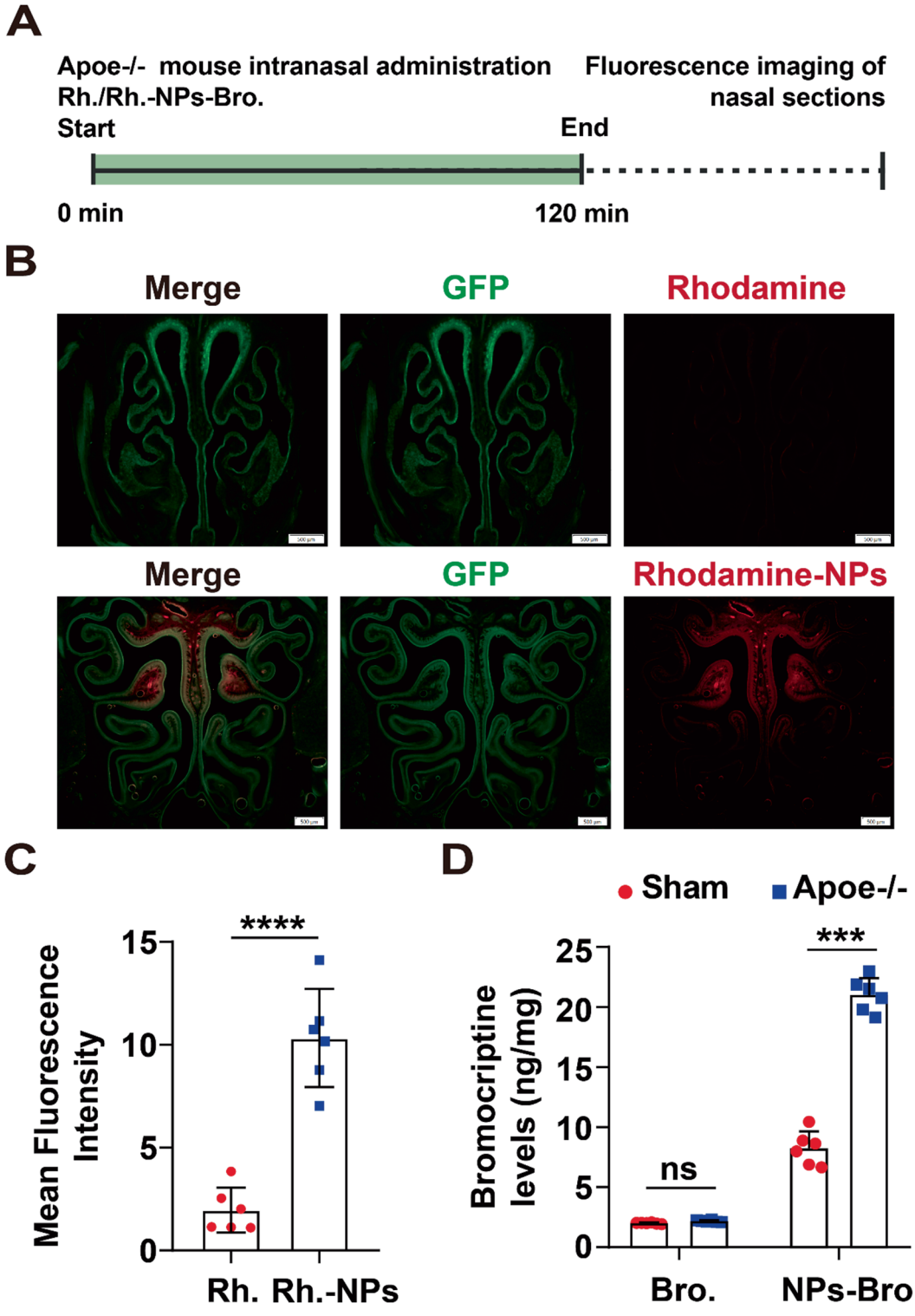

Fig. 3 Intranasal administration: Atherosclerosis enhances the delivery of NPs-Bro to the hypothalamus. (**A**) Intranasal administration of rhodamine/rhodamine-labeled nanoparticles in Apoe-/- mice during the treatment process (**B**-**C**) Rhodamine-labeled nanoparticles and statistical analysis. (**D**) Bromocriptine concentrations in the hypothalamic region, comparing free bromocriptine and liposome nanoparticle-loaded bromocriptine. (*, $P < 0.05$; **, $P < 0.01$; ***, $P < 0.001$)

we established an atherosclerotic mouse model (Apoe-/-) and analyzed 19,383 cerebral vascular cells from Sham mice and 8,473 cells from Apoe-/- mice, constructing a cellular atlas of the mouse brain microvasculature (Fig. 4A). Based on the expression of cell-type-specific markers, we identified and validated the distribution of each cellular subset (Fig. 4B-C). The results revealed 11 distinct cell types, including Endothelial cells (Pecam1, Adgrl4), Fibroblasts (Dcn, Col3a1), Vascular Smooth Muscle Cells (Acta2, Thsd4), Macrophages (C1qa, Lyz2), T cells (Cd3d, Cd3g), Astrocytes (Atp1a2), Dendritic Cells (Cd14, Cd83), Mast cells (Kit, Tpsb2), B cells (Inpp5d, Cd79a, Cd79b), Oligodendrocytes (Mbp, Gpm6b), and Granulocytes (S100a9, S100a8). Overall, the single-cell transcriptomic atlas of cerebral vasculature in Sham and Apoe-/- mice reveals the distribution of cell types within the cerebral vasculature under atherosclerotic conditions and potential changes in cellular composition, providing cellular-level evidence for studying the effects of atherosclerosis on the brain vasculature.

Enhanced NPs-Bro drug delivery in atherosclerosis is attributed to endothelial hyperproliferatio

In the constructed single-cell transcriptomic atlas of the murine cerebrovasculature, we identified pronounced alterations across 11 distinct cell types (Fig. 5A; Supplementary Fig. 3). Notably, brain vascular endothelial cells were markedly increased in Apoe$^{-/-}$ mice (Fig. 5B). These findings reflect significant shifts in cerebrovascular cell composition between non-atherosclerotic and atherosclerotic mice and reveal abnormal endothelial cell proliferation. We next performed a focused analysis of gene expression in the proliferative endothelial cell population to elucidate the mechanisms by which atherosclerosis enhances NPs_Bro drug delivery.

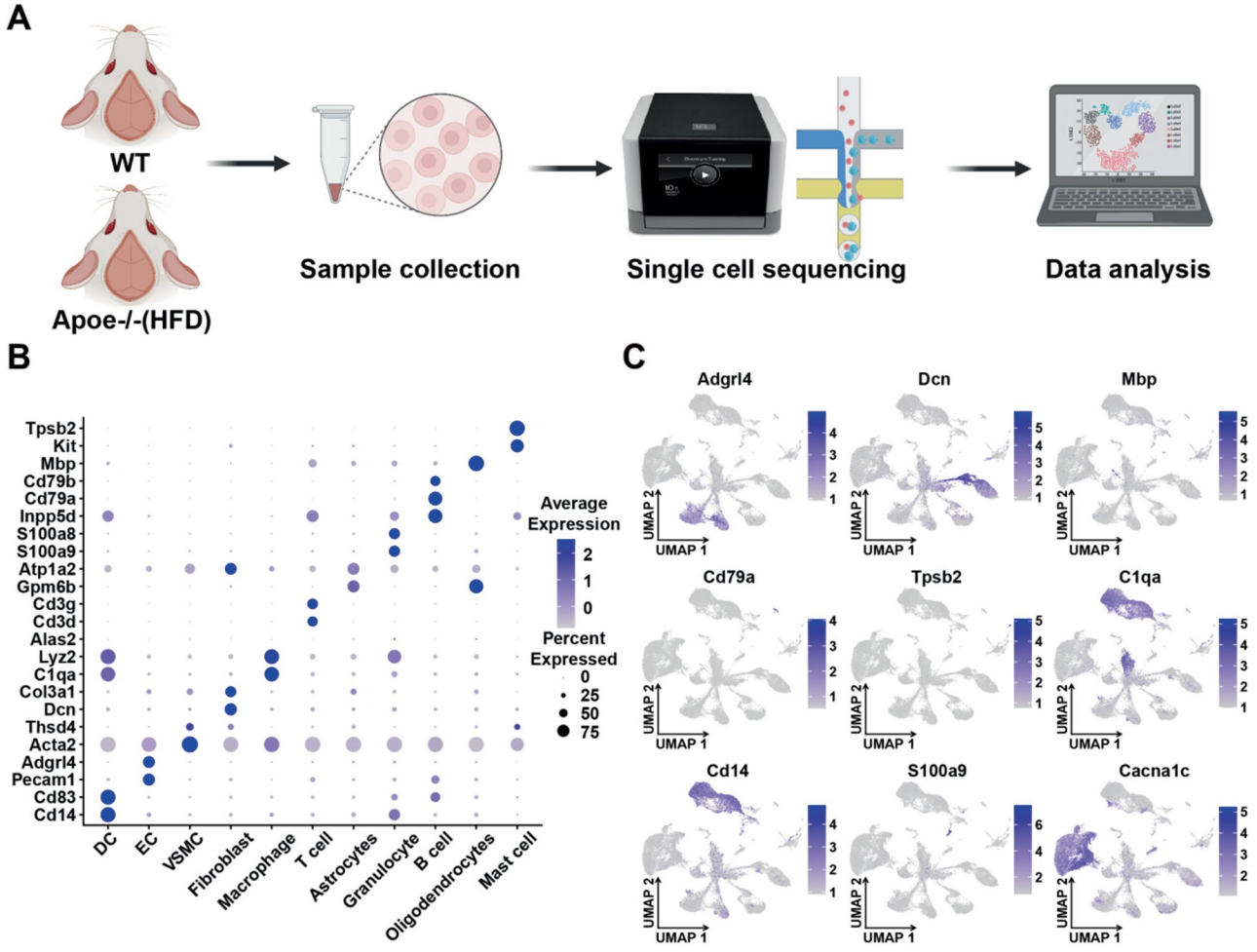

Fig. 4 Construction of a single-cell transcriptomic atlas of mouse cerebrovascular cells. (**A**) Schematic representation of the single-cell sequencing study design. Brain microvessels were isolated from mice and dissociated into single-cell suspensions for scRNA sequencing using the 10x Genomics platform. The resulting single-cell transcriptomic data were then analyzed comprehensively. Sham: WT mice; Apoe-/-: Atherosclerotic mice. (**B**) Dot plot illustrating the average expression levels of known cell markers. Dot size represents the percentage of cells within each cell type that express the indicated genes. (**C**) UMAP visualization displays selected marker genes' expression levels in 12,085 unclassified cerebrovascular cells from Sham and Apoe-/- mice

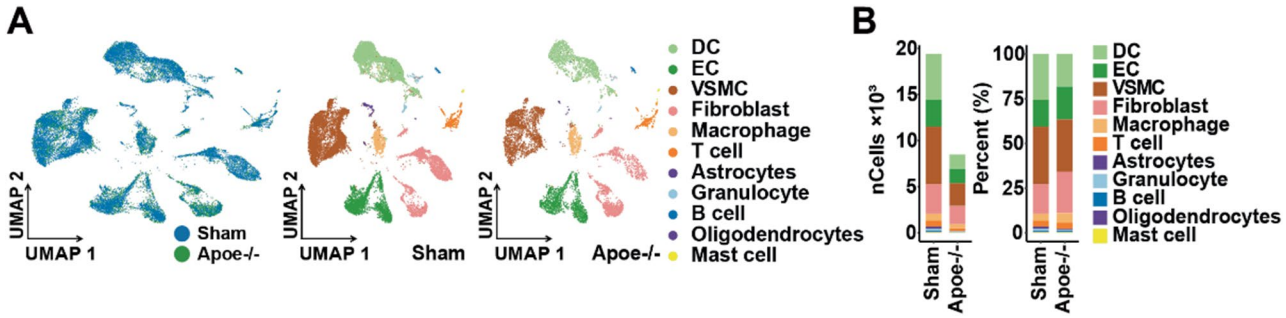

Fig. 5 Endothelial cell expansion in Apoe-/- mice cerebrovascular cells. (**A**) UMAP plots of 11 major cerebrovascular cell types from Sham and Apoe-/- mice. (**B**) Bar graph showing the number and relative proportion of clustered cerebrovascular cell types. Sham: WT mice; Apoe-/-: Atherosclerotic mice

Oatp1a4 is highly expressed in hyperproliferative endothelial cells in atherosclerotic mice

To investigate the functional heterogeneity of hyperproliferative endothelial cells in the cerebrovasculature of atherosclerotic mice, we performed clustering analysis on all endothelial cells from the brain microvasculature of Sham and Apoe-/- mice. This analysis identified six distinct endothelial subpopulations (EC_1, EC_2, EC_3, EC_4, EC_5, and EC_6) (Fig. 6A). Notably, in the Apoe-/- group, the proportions of EC_1, EC_2, and EC_5 were increased, whereas EC_3, EC_4, and EC_6 were significantly reduced (Fig. 6B). To characterize these subpopulations, we identified marker genes distinguishing each cluster (Fig. 6C). Gene Ontology (GO) enrichment analysis of the significantly expanded EC_1, EC_2, and EC_5 subpopulations revealed enrichment in expected biological processes. Interestingly, GO analysis of highly expressed genes in the EC_2 subpopulation indicated a strong association with biological transmembrane transporter activity, active transmembrane transporter activity, and biotin transmembrane transporter activity (Supplementary Fig. 4). To investigate the differences in substance transport following endothelial cell disruption, we focused on the TOP genes of the EC_2 subset. We found that organic anion-transporting polypeptide 1a4 (Oatp1a4) was significantly upregulated (Fig. 6D, Supplementary Fig. 5). Consistently, compared to Sham mice, Oatp1a4 expression was higher in Apoe-/- mice (Fig. 6E). Previous studies have shown that Oatp1a4 is expressed at the blood-brain barrier (BBB) in mice, facilitating the transport of statins across the BBB and contributing to improved neurocognitive outcomes following atherosclerotic thrombotic stroke [29, 30]. We isolated cerebral microvessels from adult mice and performed immunostaining to determine the distribution of Oatp1a4 in the brains of non-atherosclerotic and atherosclerotic mice. The results confirmed that Oatp1a4 was localized to endothelial cells (Fig. 6F). Our findings suggest that the increased expression of Oatp1a4 in the BBB of atherosclerotic mice may play a crucial role in NPs_Bro drug delivery, potentially enhancing therapeutic efficacy in these models.

NPs-Bro effectively reduces prolactin levels in atherosclerotic mice

We established a prolactinoma model using estradiol benzoate treatment to evaluate the therapeutic efficacy of intranasally administered NPs-Bro in Apoe-/- mice (Fig. 7A). Following 30 days of continuous intranasal administration, we assessed prolactin levels using an ELISA kit. Our results demonstrated that NPs-Bro effectively reduced prolactin levels, with a more pronounced effect in Apoe-/- mice (Fig. 7B-C). Additionally, we established a hyperprolactinemia model using sulpiride administration (Fig. 7D). Following 30 days of continuous intranasal delivery, NPs-Bro effectively reduced serum prolactin levels, with a more pronounced effect observed in Apoe$^{-/-}$ mice (Fig. 7E-F). These findings indicate that, compared to normal mice, liposomal nanoparticle-loaded bromocriptine more effectively reduces prolactin levels. Intranasal administration significantly enhances targeted therapeutic delivery, with this effect being more pronounced in atherosclerotic mouse models.

Furthermore, we assessed the biocompatibility of NPs-Bro. Hematoxylin and eosin (H&E) staining of major organs revealed no significant pathological changes in the NPs-Bro-treated group compared to the Sham group (Supplementary Fig. 6). The results demonstrate that NPs-Bro exhibits excellent biocompatibility.

Conclusion

This study found that liposomal-loaded bromocriptine exhibited enhanced blood-brain barrier (BBB) penetration efficiency in the atherosclerosis model and significantly improved the reduction of prolactin levels in atherosclerotic mice. Clinical data show that preoperative bromocriptine administration significantly improves surgical outcomes in patients with retinal arteriosclerosis, effectively reduces prolactin levels, and enhances the precision of prolactinoma treatment. This dual therapeutic effect provides an important clinical treatment strategy

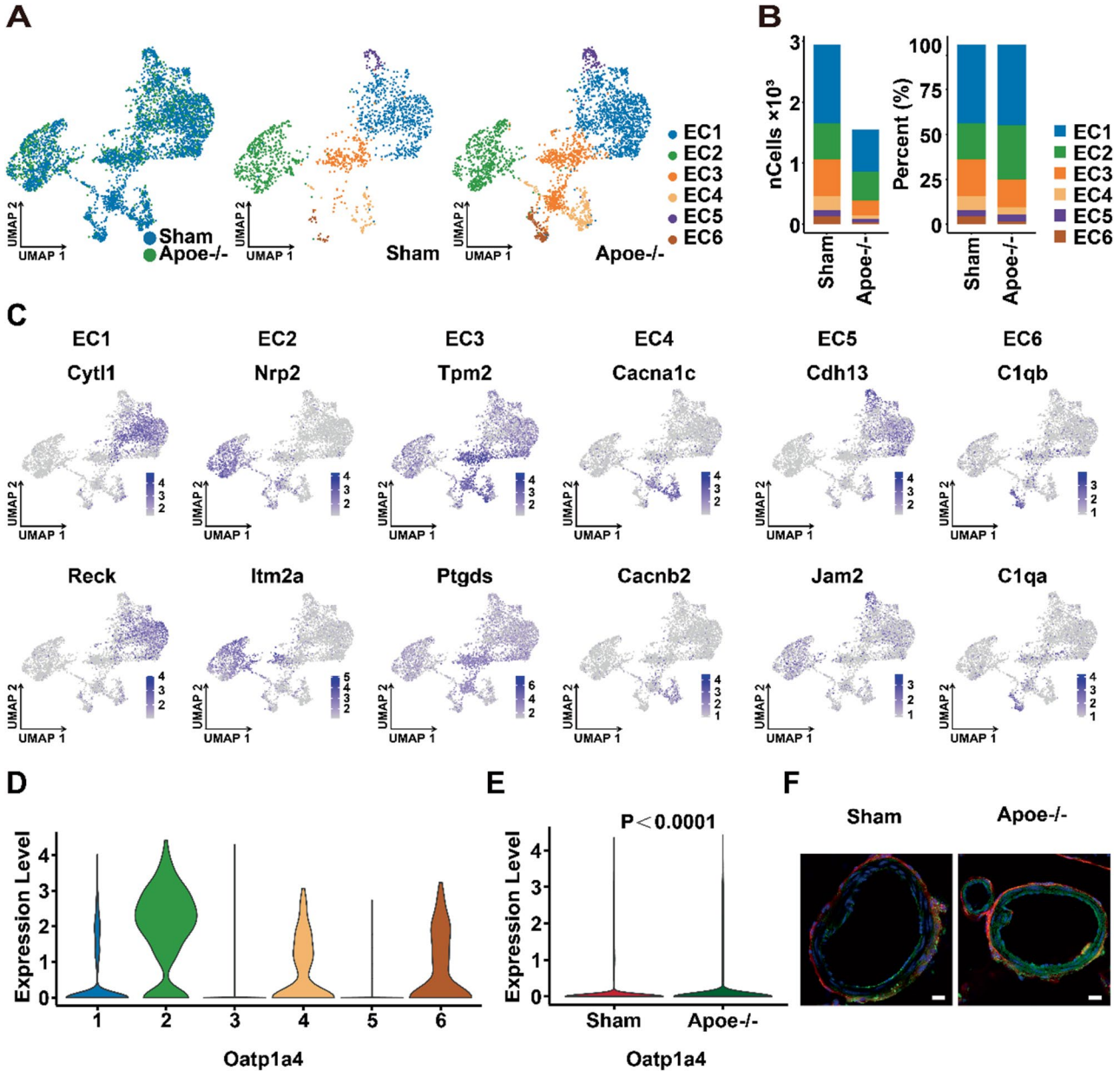

Fig. 6 Oatp1a4 is significantly expressed in hyperproliferative endothelial cells of Apoe-/- mice. (**A**) UMAP plots of EC subsets (EC_1, EC_2, EC_3, EC_4, EC_5, and EC_6) from Sham (342 cells) and ApoE-/- (886 cells) groups. (**B**) Bar graph showing the number and relative proportion of EC subsets. (**C**) UMAP plots of representative genes across the six EC subsets. (**D**) Oatp1a4 was significantly expressed in the EC_2 subset. (**E**) Oatp1a4 expression is higher in Apoe-/- mice compared to Sham mice. (**F**) Representative immunofluorescence images showing Oatp1a4 localization in the cerebrovasculature of Sham and Apoe-/- mice (green: Oatp1a4)

for prolactinoma patients with concomitant vascular sclerosis.

Materials and methods

Patient information and screening

637 patients with pituitary tumors who underwent surgical treatment at the Department of Neurosurgery, Second Affiliated Hospital of Nanchang University, were screened for eligibility from January 2018 to December 2023. Inclusion criteria: (1) confirmed prolactinoma by pathological examination; (2) serum prolactin > 2.8 ng/ml; (3) aged over 18 years; (4) fundus photography; (5) complete written informed consent. Exclusion criteria: (1) previous history of pituitary adenoma surgery; (2) history of underlying diseases (including hypertension, diabetes, heart disease, etc.); (3) incomplete preoperative or postoperative imaging data; (4) use of bromocriptine for < 6 months; (5) simultaneous use of other medications or participation in other clinical trials before surgery. Based on the results of fundus photography, 51 patients

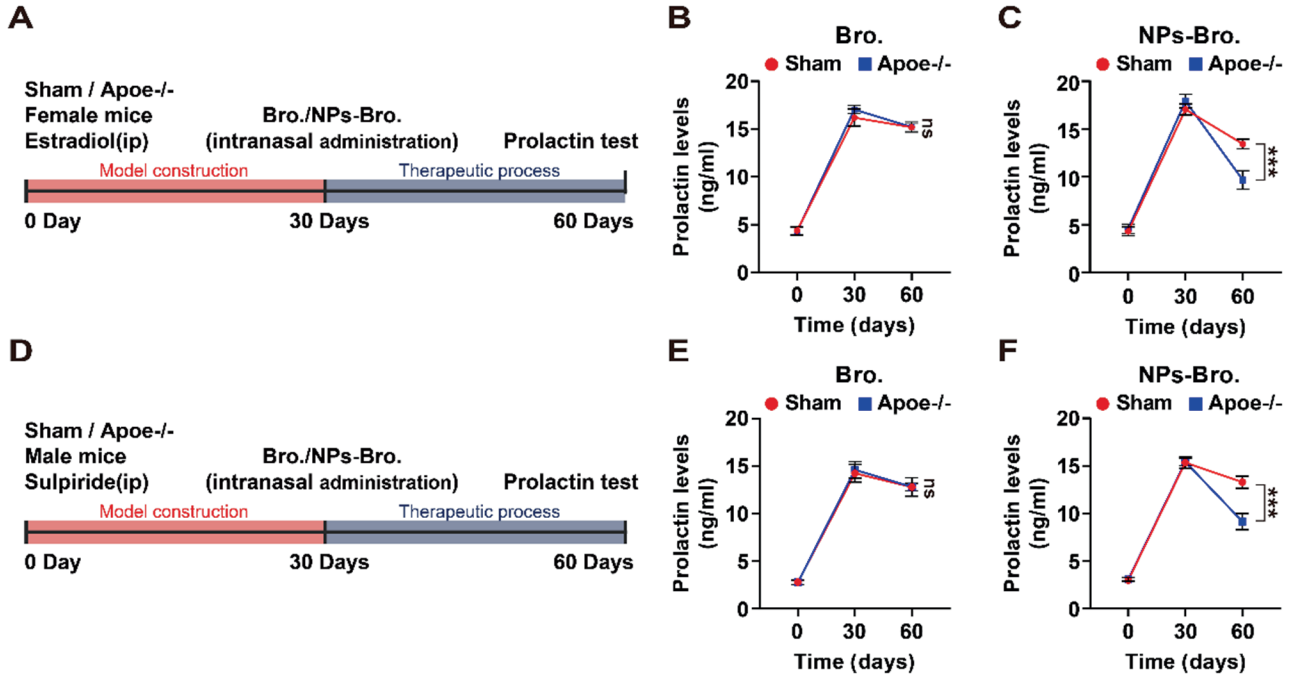

Fig. 7 Intranasal administration of NPs-Bro more effectively reduces prolactin levels in Apoe-/- mice. (**A-C**) Effects of free bromocriptine and NPs-Bro on estradiol-induced prolactinoma models in Sham and Apoe-/- mice. (**D–F**) Effects of free bromocriptine and NPs-Bro on sulpiride-induced hyperprolactinemia model in Sham and Apoe-/- mice. Bro: Bromocriptine.(*, $P < 0.05$; **, $P < 0.01$; ***, $P < 0.001$)

were assigned to the retinal arteriosclerosis group (arteriosclerosis group), 77 patients to the retinal artery normal group (non-arteriosclerosis group), and 52 patients to the unknown retinal artery status group. The arteriosclerosis group had 12 cases of hypertension and 1 case of diabetes. The non-arteriosclerosis group had 8 cases of hypertension. Patients with underlying diseases were excluded from the study. Additionally, in the arteriosclerosis group, 10 patients lacked complete imaging data, and 7 patients had not received bromocriptine treatment for more than 6 months before surgery. In the non-arteriosclerosis group, 25 patients had incomplete imaging data, and 19 patients had not received bromocriptine treatment for more than 6 months before surgery. Therefore, 21 patients from the arteriosclerosis group and 25 patients from the non-arteriosclerosis group were included in the initial phase of the study. Among them, 7 patients from the arteriosclerosis group and 16 patients from the non-arteriosclerosis group completed 6 months of follow-up and were included in the final analysis (flowchart in Supplementary Fig. 4). This study was approved by the Biomedical Research Ethics Committee of the Second Affiliated Hospital of Nanchang University (Project Approval No: O-Medical Research Ethics Review [2024] 05).

Materials

Bromocriptine and soybean lecithin containing 75% phosphatidylcholine, 2-distearoyl-sn-glycero-3-phosphoethanolamine, and sodium salt (DSPE-mPEG-2000) were purchased from Cayman Chemical Company (USA). Cholesterol was obtained from Aladdin Reagents (Shanghai, China).

Preparation and characterization

Bromocriptine liposomes were prepared using the thin-film hydration-ultrasonication method [21]. Briefly, the hydration process was performed at 65 °C using 1300 μL of deionized water for 60 min, utilizing a rotary evaporator (Heidolph, Germany), followed by sonication of the resulting nano-drug. The size and distribution of the bromocriptine-loaded liposomes were measured using a Malvern Zetasizer Nano ZS90 ζ potential analyzer (DLS, Malvern, UK) [31]. To assess the stability of the nanocarriers, the bromocriptine-loaded liposomes were incubated for 1 day at 37 °C in Dulbecco's Modified Eagle Medium (DMEM; Gibco, Carlsbad, CA) containing 10% serum (v/v), and the size of the nanocarriers was monitored.

ELISA assay

The prolactin levels were measured using an ELISA kit (ED20246, Luncanso Biotechnology Co., Ltd., Xiamen). Mouse serum samples (50 μL) were analyzed. All procedures were performed according to the manufacturer's instructions.

Animals

In this study, 12-week-old male and female wild-type (WT) mice were fed standard laboratory chow, while ApoE-/- mice (C57BL/6J, T001458, Jiangsu, China) were fed a high-fat diet [32]. C57/BL/6-Tg (UBC-GFP)30 Scha/J mice (#004353) were obtained from The Jackson Laboratory. All mice were housed in specific-pathogen-free (SPF) cages and provided autoclaved water and food.

Single-Cell RNA sequencing

Brain microvessels from 20 mice (WT and ApoE−/−) per group were carefully dissected and digested. The fresh brain vascular cell suspension was prepared following the manufacturer's protocol using the 10x Chromium 3'v3 kit (10x Genomics, 1000120) [33, 34]. Single cells were suspended in PBS containing 0.04% BSA and loaded into individual channels. The captured cells were lysed, and barcode RNA was released through reverse transcription in individual GEMs. Reverse transcription was performed on the S1000™ Touch Thermal Cycler (Bio-Rad) at 53 °C for 45 min, followed by 85 °C for 5 min, and then held at 4 °C. cDNA generation and amplification were quality-controlled using the Agilent 4200 system [35]. Sequencing was performed using the NovaSeq 6000 sequencer provided by Novogene (Beijing, China), CapitalBio Technology.

Single-Cell RNA data analysis

First, expression data were normalized using the unistandard method. Cell Ranger was used to align reads, generate feature barcode matrices, create global gene expression, and perform clustering [36]. Data dimensionality reduction, cell clustering, differential analysis, and single-cell RNA-seq data visualization were performed using the Seurat R package (version 3.0) [37]. Select those that simultaneously satisfy 200 < the number of genes; UMI < 99th percentile value; Cells with mitochondrial gene expression ratio ≤ 25%. PCA was used for dimensional reconstruction, and cell types were identified using CellMarker, with UMAP used for visualization analysis. Functional enrichment analysis was conducted using the Gene Ontology Consortium and Kyoto Encyclopedia of Genes and Genomes [38–40].

Western blotting

Protein expression levels of Bax, Bcl-2, and OATP were assessed by Western blotting. Collected protein samples were separated by SDS-PAGE and transferred onto polyvinylidene difluoride (PVDF) membranes (USA). Primary antibodies used included Bax (ab182733), Bcl-2 (ab182858), OATP (ab221804), as well as internal controls GAPDH and Tubulin. Appropriate secondary antibodies were applied accordingly. All of the blots were repeated at least three times.

Cell culture and ox-LDL-Induced injury model

Human cerebral microvascular endothelial cell line (hCMEC/D3) and astrocytes were obtained from the Shanghai Cell Bank of the Chinese Academy of Sciences. Cells were cultured in an incubator at 37 °C, 95% humidity, and 5% CO2, with the culture medium supplemented with 10% fetal bovine serum (FBS) and 1% penicillin/streptomycin. hCMEC/D3 cells were treated with different concentrations of ox-LDL (20, 40, 60, 80 μg/ml, Union-Bio Technology, China) and collected after 24 h. To evaluate the successful establishment of an in vitro atherosclerosis cell model, we investigated the effects of oxidized low-density lipoprotein (ox-LDL) on the proliferation and apoptosis of hCMEC/D3 cells. Cell viability was assessed using the CCK-8 assay (Solarbio, China) according to the manufacturer's instructions. We observed a dose-dependent decrease in cell viability upon exposure to ox-LDL (0–80 μg/mL) (Supplementary Fig. 7A). Ox-LDL exposure also enhanced apoptosis, as evidenced by reduced Bcl-2 expression and increased Bax expression (Supplementary Fig. 7B–D). OATP1A2, the human homolog of Slco1a4, was examined to assess its expression under ox-LDL conditions. Western blot analysis revealed a marked upregulation of OATP1A2 expression in response to increasing levels of cellular injury (Supplementary Fig. 7E–F).

Animal models

A prolactinoma mouse model was established using estradiol benzoate (HY-B0141, MCE) in female WT/Apoe−/− mice ($n = 12$ per group). Estradiol benzoate (20 mg/kg) was intraperitoneally injected every 2 days for 30 days, successfully creating the prolactinoma model in mice [41]. A hyperprolactinemia mouse model was established using sulpiride (HY-B1019, MCE) in male WT and $ApoE^{-/-}$ mice ($n = 12$ per group). Sulpiride was administered via intraperitoneal injection at a dose of 20 mg/kg once daily for 30 consecutive days to induce hyperprolactinemia [42]. The established model group mice were randomly assigned to two treatment groups: Bromocriptine ($n = 12$) and NPs + Bromocriptine ($n = 12$).

Liquid Chromatography-Tandem mass spectrometry (LC-MS/MS)

Liquid chromatography-tandem mass spectrometry (LC-MS/MS) was employed to quantitatively determine the concentration of bromocriptine (HY-12705 A, MCE) in brain tissue and cell samples. First, an accurate amount of bromocriptine was weighed and dissolved in methanol to prepare a stock solution of 2.00 mg/mL. The stock solution was diluted with pure methanol to create a standard curve working solution of 200 ng/mL. The hypothalamus was carefully dissected to analyze brain tissue, and an appropriate amount of tissue was weighed. The tissue was

then homogenized in methanol using vortex mixing and bead milling for 5 min. The sample was then subjected to high-speed centrifugation at 13,000 rpm for 10 min. The supernatant was filtered through a 0.22 μm filter before being subjected to analysis [43]. Chromatographic data collection and processing were carried out using Xcalibur software (Thermo Fisher), with linear regression performed using Equal as the weight factor [44].

Immunofluorescence staining and imaging

Brain tissue sections were prepared at a thickness of 20 μm using a cryostat for immunofluorescence staining. After blocking, the sections were incubated overnight at 4 °C with the appropriately diluted primary antibody against Oatp1a4 (sc-376424, 1:100). After three washes, the sections were incubated at room temperature for 4 h with the FITC (green)-conjugated secondary antibody. Imaging was performed using a Leica DMi8 confocal microscope and LAS AF software (Leica Microsystems).

Statistical analysis

Statistical analyses were performed using SPSS (IBM) and Prism 8 (GraphPad Software). A two-tailed, unpaired Student's t-test was used to evaluate the statistical significance between the two groups. A P-value of less than 0.05 was considered statistically significant.

Supplementary Information

The online version contains supplementary material available at https://doi.org/10.1186/s12951-025-03465-0.

Supplementary Material 1

Author contributions

ZZ, GYJ, and QW contributed equally to this work. ZZ, YMY, and SYL completed the experimental conception and design. Clinical data were collected by YX, JJJ, and YRO. GYJ, XLT, and QW provided technical support for scRNA-Seq data analysis. HQZ and XYY did review and editing. HG and YW supervised this study.

Funding

This work was supported by the National Natural Science Foundation of China (82471354 and 82171335), High-End Talent Program for Science and Technology Innovation - Natural Sciences Category (G3422), Science and Technology Program of Jiangxi Province, China (20224ACB206017, 20213BCJ22012).

Data availability

No datasets were generated or analysed during the current study.

Declarations

Ethics approval and consent to participate

All mouse experiments were conducted following the Guidelines for the Care and Use of Laboratory Animals and approved by the Animal Ethics Committee of Nanchang University.

Consent for publication

All authors read and approved the final manuscript.

Competing interests

The authors declare no competing interests.

Author details

[1]Department of Neurosurgery, The Second Affiliated Hospital, Jiangxi Medical College, Nanchang University, Nanchang, Jiangxi, China
[2]Department of Neurology, The Second Affiliated Hospital, Jiangxi Medical College, Nanchang University, Nanchang, Jiangxi, China
[3]Jiangxi Key Laboratory of Neurological Tumors and Cerebrovascular Diseases, Nanchang, Jiangxi, China
[4]Institute of Neuroscience, Nanchang University, Nanchang, Jiangxi, China
[5]Jiangxi Province Key Laboratory of Neurological Diseases, Nanchang, Jiangxi, China
[6]JXHC Key Laboratory of Neurological Medicine, Nanchang, Jiangxi, China

Received: 15 March 2025 / Accepted: 14 May 2025
Published online: 29 May 2025

References

1. Michael Besser G, Pfeiffer RF, Thorner MO. ANNIVERSARY REVIEW: 50 years since the discovery of Bromocriptine. Eur J Endocrinol. 2018;179:R69–75.
2. Gittleman H, Ostrom QT, Farah PD, Ondracek A, Chen Y, Wolinsky Y, Kruchko C, Singer J, Kshettry VR, Laws ER, et al. Descriptive epidemiology of pituitary tumors in the united States, 2004–2009. J Neurosurg. 2014;121:527–35.
3. Tritos NA, Miller KK. Diagnosis and management of pituitary adenomas: A review. JAMA. 2023;329:1386–98.
4. Liu Y, Su W, Liu Z, Hu Z, Shen J, Zheng Z, Ding D, Huang W, Li W, Cai G, et al. Macrophage CREBZF orchestrates inflammatory response to potentiate insulin resistance and type 2 diabetes. Adv Sci (Weinh). 2024;11:e2306685.
5. Ben-Jonathan N. Dopamine: a prolactin-inhibiting hormone. Endocr Rev. 1985;6:564–89.
6. Jackson DM, Westlind-Danielsson A. Dopamine receptors: molecular biology, biochemistry and behavioural aspects. Pharmacol Ther. 1994;64:291–370.
7. Zhang S, Ji X, Liu Z, Xie Z, Wang Y, Wang H, Ni D. Bimetallic nanoplatforms for prostate Cancer treatment by interfering cellular communication. J Am Chem Soc. 2024;146:22530–40.
8. Li S, Jiang D, Ehlerding EB, Rosenkrans ZT, Engle JW, Wang Y, Liu H, Ni D, Cai W. Intrathecal administration of nanoclusters for protecting neurons against oxidative stress in cerebral ischemia/reperfusion injury. ACS Nano. 2019;13:13382–9.
9. Wu D, Chen Q, Chen X, Han F, Chen Z, Wang Y. The blood-brain barrier: structure, regulation, and drug delivery. Signal Transduct Target Ther. 2023;8:217.
10. Jackson S, Meeks C, Vézina A, Robey RW, Tanner K, Gottesman MM. Model systems for studying the blood-brain barrier: applications and challenges. Biomaterials. 2019;214:119217.
11. Laffleur F, Bauer B. Progress in nasal drug delivery systems. Int J Pharm. 2021;607:120994.
12. Ugwoke MI, Agu RU, Verbeke N, Kinget R. Nasal mucoadhesive drug delivery: background, applications, trends and future perspectives. Adv Drug Deliv Rev. 2005;57:1640–65.
13. Allen TM, Cullis PR. Liposomal drug delivery systems: from concept to clinical applications. Adv Drug Deliv Rev. 2013;65:36–48.
14. Yuan Z, Gottsacker C, He X, Waterkotte T, Park YC. Repetitive drug delivery using Light-Activated liposomes for potential antimicrobial therapies. Adv Drug Deliv Rev. 2022;187:114395.
15. Wang H, Hsu JC, Song W, Lan X, Cai W, Ni D. Nanorepair medicine for treatment of organ injury. Natl Sci Rev. 2024;11:nwae280.
16. Zhan R, Zhao M, Zhou T, Chen Y, Yu W, Zhao L, Zhang T, Wang H, Yang H, Jin Y, et al. Dapsone protects brain microvascular integrity from high-fat diet induced LDL oxidation. Cell Death Dis. 2018;9:683.
17. Tan J, Liang Y, Yang Z, He Q, Tong J, Deng Y, Guo W, Liang K, Tang J, Shi W, Yu B. Single-Cell transcriptomics reveals crucial cell subsets and functional heterogeneity associated with carotid atherosclerosis and cerebrovascular events. Arterioscler Thromb Vasc Biol. 2023;43:2312–32.
18. Barabási B, Barna L, Santa-Maria AR, Harazin A, Molnár R, Kincses A, Vigh JP, Dukay B, Sántha M, Tóth ME, et al. Role of interleukin-6 and interleukin-10 in morphological and functional changes of the blood-brain barrier in hypertriglyceridemia. Fluids Barriers CNS. 2023;20:15.

19. Seferović PM, Polovina M. The eyes are the mirror of the heart: role of retinal microvascular abnormalities in predicting long-term risk of heart failure. Eur J Heart Fail. 2019;21:1216–8.
20. Seferović PM, Polovina M, Bauersachs J, Arad M, Ben Gal T, Lund LH, Felix SB, Arbustini E, Caforio ALP, Farmakis D, et al. Heart failure in cardiomyopathies: a position paper from the heart failure association of the European society of cardiology. Eur J Heart Fail. 2019;21:553–76.
21. Sheikhpour M, Sadeghizadeh M, Yazdian F, Mansoori A, Asadi H, Movafagh A, Shahraeini SS. Co-Administration of Curcumin and Bromocriptine Nanoliposomes for induction of apoptosis in lung Cancer cells. Iran Biomed J. 2020;24:24–9.
22. Zheng H, Pei Y, Zhou C, Hong P, Qian ZJ. Amelioration of atherosclerosis in ox-LDL induced HUVEC by sulfated polysaccharides from Gelidium crinale with antihypertensive activity. Int J Biol Macromol. 2023;228:671–80.
23. Wang ZC, Niu KM, Wu YJ, Du KR, Qi LW, Zhou YB, Sun HJ. A dual Keap1 and p47(phox) inhibitor ginsenoside Rb1 ameliorates high glucose/ox-LDL-induced endothelial cell injury and atherosclerosis. Cell Death Dis. 2022;13:824.
24. Lochhead JJ, Thorne RG. Intranasal delivery of biologics to the central nervous system. Adv Drug Deliv Rev. 2012;64:614–28.
25. Chen Y, Zhang C, Huang Y, Ma Y, Song Q, Chen H, Jiang G, Gao X. Intranasal drug delivery: the interaction between nanoparticles and the nose-to-brain pathway. Adv Drug Deliv Rev. 2024;207:115196.
26. Crowe TP, Hsu WH. Evaluation of recent intranasal drug delivery systems to the central nervous system. Pharmaceutics 2022;14.
27. Papalexi E, Satija R. Single-cell RNA sequencing to explore immune cell heterogeneity. Nat Rev Immunol. 2018;18:35–45.
28. Winkler EA, Kim CN, Ross JM, Garcia JH, Gil E, Oh I, Chen LQ, Wu D, Catapano JS, Raygor K, et al. A single-cell atlas of the normal and malformed human brain vasculature. Science. 2022;375:eabi7377.
29. Ronaldson PT, Davis TP. Targeted drug delivery to treat pain and cerebral hypoxia. Pharmacol Rev. 2013;65:291–314.
30. Gao B, Vavricka SR, Meier PJ, Stieger B. Differential cellular expression of organic anion transporting peptides OATP1A2 and OATP2B1 in the human retina and brain: implications for carrier-mediated transport of neuropeptides and neurosteriods in the CNS. Pflugers Arch. 2015;467:1481–93.
31. Wang Y, Li SY, Shen S, Wang J. Protecting neurons from cerebral ischemia/reperfusion injury via nanoparticle-mediated delivery of an SiRNA to inhibit microglial neurotoxicity. Biomaterials. 2018;161:95–105.
32. Zhang Y, Jiang H, Dong M, Min J, He X, Tan Y, Liu F, Chen M, Chen X, Yin Q, et al. Macrophage MCT4 Inhibition activates reparative genes and protects from atherosclerosis by histone H3 lysine 18 lactylation. Cell Rep. 2024;43:114180.
33. Scheyltjens I, Van Hove H, De Vlaminck K, Kancheva D, Bastos J, Vara-Pérez M, Pombo Antunes AR, Martens L, Scott CL, Van Ginderachter JA, et al. Single-cell RNA and protein profiling of immune cells from the mouse brain and its border tissues. Nat Protoc. 2022;17:2354–88.
34. Li Y, Li F, Xu L, Shi X, Xue H, Liu J, Bai S, Wu Y, Yang Z, Xue F, et al. Single cell analyses reveal the PD-1 Blockade response-related immune features in hepatocellular carcinoma. Theranostics. 2024;14:3526–47.
35. Li F, Yan K, Wu L, Zheng Z, Du Y, Liu Z, Zhao L, Li W, Sheng Y, Ren L, et al. Single-cell RNA-seq reveals cellular heterogeneity of mouse carotid artery under disturbed flow. Cell Death Discov. 2021;7:180.
36. Yu D, Huber W, Vitek O. Shrinkage Estimation of dispersion in negative binomial models for RNA-seq experiments with small sample size. Bioinformatics. 2013;29:1275–82.
37. Stuart T, Butler A, Hoffman P, Hafemeister C, Papalexi E, Mauck WM 3rd, Hao Y, Stoeckius M, Smibert P, Satija R. Comprehensive integration of Single-Cell data. Cell. 2019;177:1888–e19021821.
38. Kanehisa M, Goto S. KEGG: Kyoto encyclopedia of genes and genomes. Nucleic Acids Res. 2000;28:27–30.
39. Ashburner M, Ball CA, Blake JA, Botstein D, Butler H, Cherry JM, Davis AP, Dolinski K, Dwight SS, Eppig JT, et al. Gene ontology: tool for the unification of biology. The gene ontology consortium. Nat Genet. 2000;25:25–9.
40. Aleksander SA, Balhoff J, Carbon S, Cherry JM, Drabkin HJ, Ebert D, Feuermann M, Gaudet P, Harris NL, Hill DP et al. The gene ontology knowledgebase in 2023. Genetics 2023;224.
41. Ding QY, Zhang Y, Ma L, Chen YG, Wu JH, Zhang HF, Wang X. Inhibiting MAPK14 showed anti-prolactinoma effect. BMC Endocr Disord. 2020;20:138.
42. Adán-Castro E, Siqueiros-Márquez L, Ramírez-Hernández G, Díaz-Lezama N, Ruíz-Herrera X, Núñez FF, Núñez-Amaro CD, Robles-Osorio ML, Bertsch T, Triebel J, et al. Sulpiride-induced hyperprolactinaemia increases retinal vasoinhibin and protects against diabetic retinopathy in rats. J Neuroendocrinol. 2022;34:e13091.
43. Li XS, Li S, Wynveen P, Mork K, Kellermann G. Development and validation of a specific and sensitive LC-MS/MS method for quantification of urinary catecholamines and application in biological variation studies. Anal Bioanal Chem. 2014;406:7287–97.
44. Tie C, Hu T, Jia ZX, Zhang JL. Derivatization strategy for the comprehensive characterization of endogenous fatty aldehydes using HPLC-Multiple reaction monitoring. Anal Chem. 2016;88:7762–8.

Publisher's note